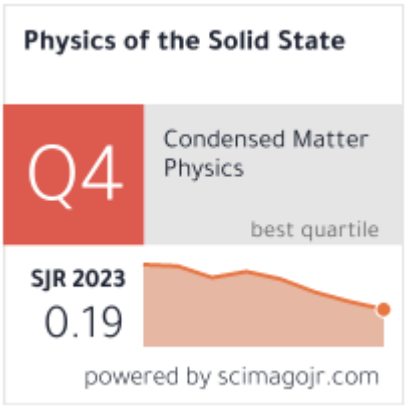

Physics of the Solid State

COUNTRY	SUBJECT AREA AND CATEGORY	PUBLISHER	H-INDEX
United States Universities and research institutions in United States Media Ranking in United States	Materials Science └ Electronic, Optical and Magnetic Materials Physics and Astronomy └ Condensed Matter Physics	Pleiades Publishing	56

PUBLICATION TYPE	ISSN	COVERAGE	INFORMATION
Journals	10637834, 10906460	1996-2023	Homepage How to publish in this journal sst@journals.ioffe.rssi.ru

SCOPE

Presents the latest results from Russia's leading researchers in condensed matter physics at the Russian Academy of Sciences and other prestigious institutions. Covers all areas of solid state physics including solid state optics, solid state acoustics, electronic and vibrational spectra, phase transitions, ferroelectricity, magnetism, and superconductivity. Also presents review papers on the most important problems in solid state physics.

Join the conversation about this journal

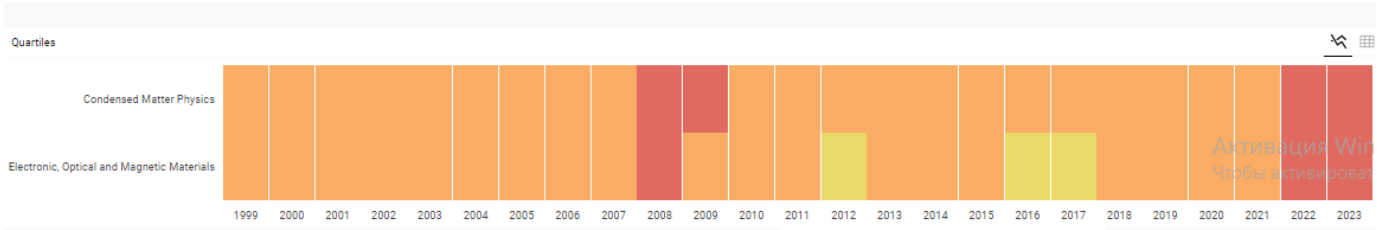

ISSN 1063-7834, Physics of the Solid State, 2024, Vol. 66, No. 2, pp. 42–50. © Pleiades Publishing, Ltd., 2024.
Russian Text © The Author(s), 2023, published in Prikladnaya Fizika i Matematika, 2023, No. 5, pp. 35–45.

Thermal and Diffusion Processes during Electron Beam Processing of Surfaces of Electroexplosive Alloying

A. V. Ionina[a,*]

[a] *Branch of Kuzbass State Technical University named after T. F. Gorbachev, Kemerovo, 654006 Russia*

**e-mail: @@@*

Received February 28, 2024; revised April 1, 2024; accepted April 1, 2024

Abstract—The mechanisms of hardening surface layers of carbon steel 45 after combined treatment including electroexplosive boroaluminizing, aluminizing with silicon carbide, and electron beam processing (EBP) are revealed. The combined processing leads to an increase in the hardening depth. After the electroexplosive boroaluminizing and EBP, the microhardeness is 16 GPa and the hardening depth is 90 μm; after the electroexplosive aluminizing combined with silicon carbide and EBP, the microhardness is 12.5 GPa and the hardening depth is 50 μm. In the initial state, the microhardness is 2 GPa. In the conditions of dry sliding friction, the wear resistance increases by a factor of 43 after electroexplosive boroaluminizing and EBP, and by a factor of 12 after electroexplosive aluminizing with silicon carbide. The surface hardening is achieved as a result of the formation of fine-disperse nonequilibrium structure containing strengthening phases. The models developed in this work allow one to explain the results by the peculiarities of the thermal and diffusion processes during EBP.

Keywords: surface hardening, electroexplosive alloying, wear resistance, dislocation substructure, hardening mechanisms, microhardness

DOI: 10.1134/S1063783424600523

INTRODUCTION

Surface hardening of metals and alloys using concentrated energy fluxes (CEF) is developed at a higher pace than traditional technologies of thermal and thermochemical treatments [1]. In recent decades, new method of such treatment, namely, electroexplosive alloying (EEA) developed [2]. It is a modification of the structure and properties of surface layers of materials by the formation of pulsed multiphase plasma jets during electric explosion of conductors, the surface melting with plasma jets and the saturation of the melt with explosion products with subsequent self-quenching and the formation of new phases and compounds.

In some cases, EEA allows us to obtain the structural–phase states unattainable when using other similar treatment methods and having high functional properties on the surface of an irradiated material. According to [3, 4, 19], around 90% of emergence breakdowns of vehicles occur due to wear, corrosion, high-temperature oxidation and other causes, and the costs of repair and maintenance of these machines are several times higher than their cost. 80% of the total downtime in industry is associated with these factors, and 20% of the metal smelted annually is spent on the manufacture of spare parts. At the same time, the inhomogeneity of the plasma jet structure and also the pulsed character of the thermal force effect on the surface during EEA are the reasons of the formation of a high-developed relief of the irradiated surface and the incompleteness of structural–phase transformations in the alloying zone. This fact can restrict the possibilities of applying this method in practice.

Recent studies [5–12] showed that the possibilities of EEA can be improved as it is used in combination with electron-beam processing (EBP) that is carried out with melting of the surface by low-energy high-current electron beams (LEHCEB). Such a combined treatment leads to equating the surface, an increase in the hardening zone depth and enhancing the functional properties of the hardening zone.

The aim of this work is to reveal the regularities of the formation of surface layers to enhance the functional properties of surface layers of carbon steel 45 by EBP of the steel 45 surface after electroexplosive boron aluminizing and aluminizing combined with silicon carbide.

EXPERIMENTAL

Steel 45 was chosen for studying the processing method, since it is widely used in industry for manufacturing tools intended for processing materials under pressure (stamps, dies, etc.). Thus, the steel must have increased wear resistance. In addition, steel 45 is com-

paratively inexpensive. The two-component electroexplosive boroaluminizing and aluminizing combined with silicon carbide was carried out placing weights of amorphous boron powder with mass 60 mg and silicon carbide powder with mass 7.5 mg, respectively, to the explosion region. Falling into a melt, submicron silicon carbide particle partially dissolve and are distributed homogeneously over the volume reinforcing the alloying zone.

To measure the layer thickness and grain sizes, to study the phase distribution in the alloying zone depth, and to photograph metallographic sections, we used a Neophot-21 metallographic microscope. This microscope allows us to obtain images of fine objects and their parts at various magnifications up to 2000.

The thin foils were prepared from the intermediate (between the central and periphery) alloying zone region at the distance 10–15 mm from its center, where its thickness reaches 20–25 μm in chosen processing conditions. To do this, the plates cut in parallel to the processed alloying zone surface by the electric-spark erosion method were thinned electrolitically. The electric discharge machining (EDM) led to surface melting and to distortion of the material structure at a depth to 100–150 μm. To eliminate its influence on the results of the studies, first plates with thickness of 450–500 μm were cut from the sample after EEA; then, the plates were ground on a thin abrasive paper to thickness of 80–100 μm and were thinned electrolitically preparing foil portions with thickness of 0.1–0.2 μm. We used the electrolyte with composition: 450 mL sulfur acid and 50 g chromium anhydride. During polishing that takes 10–30 min, the electrolyte temperature increases from room temperature to the boiling temperature. In order to reach required depth of the impact zone, we used the method of one-side thinning: first, a required thickness was removed from one side and then from the reverse side. The plate thickness was measured by a micrometer.

One of the most correct and sensitive methods of analyzing physicomechanical properties of the structure of composing materials is the microhardness measurement [13]. The difference in the microhardness before and after a treatment can be indicators of hardening of surface layers of metals and alloys. In this work, the *HV* microhardness was measured by indentation of a Vickers indenter on a PMT-3 microhardness tester at a load of 0.98 N. Its value was calculated by the results of measuring the diagonals of ten indentations. In this case, the measurement accuracy was 7–10%.

To estimate the increase in the wear resistance of the samples after EEA with respect to the samples in the initial state, we used a simple method of model wearing tests under conditions of dry sliding friction without lubrication. A ball made of quenched ShKh15 steel 15 mm in diameter rotating at a rate of 2 rev/s was applied to the sample and produced an indentation on it. The tests were periodically stopped and measured the indentation diameter *d* under an MBS-9 optical microscope. This testing method at which the area of contact of the ball with the sample continuously increases and the specific pressure on the surface is changed, and the wearing is practically stopped on reaching a certain indentation diameter is convenient for determination of the wear resistance of thin alloyed layers. In the case of such tests, the wear is expressed as the ratio of the produced indentation volume determined by its diameter to the pressure force applied to the surface from the ball and the friction path.

RESULTS AND DISCUSSION

Processing of the Aluminizing Surface

The distribution of the microhardness in the depth of steel 45 hardened layers in annealed state shows that EEA and EBP without EEA leads to close results of the hardening (Fig. 1). They are accompanied by an increase in the microhardness of the sample surface by a factor of approximately four as compared to the base. The microhardness decreases monotonically with the distance from the processing surface, changing from the maximum value 8.3 GPa to 2 GPa in the base, and it corresponds to the microhardness of the initial state at a depth of 20–25 μm.

After boroaluminizing the microhardness at the surface reaches 14.5 GPa at the alloying zone depth of 26 μm and the heat affected zone depth 17 μm. After

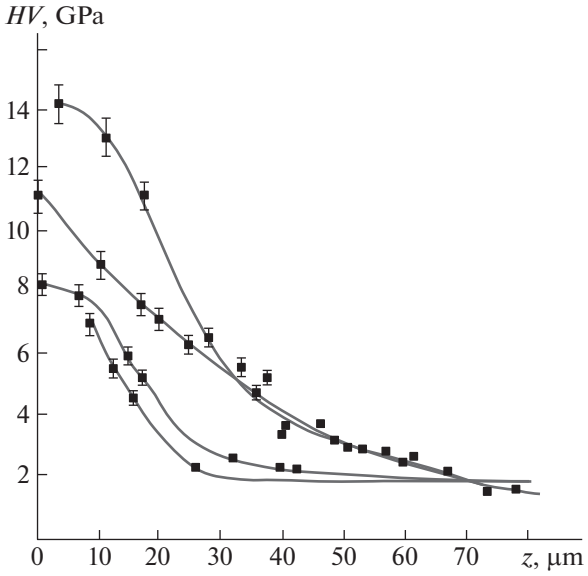

Fig. 1. Microhardness distribution over steel 45 hardened layers after various types of EEA: (*1*) EBP without EEA, (*2*) electroexplosive boroaluminizing without EBP, (*3*) electroexplosive aluminizing without EBP, (*4*) aluminizing with ultradisperse silicon carbide without EBP.

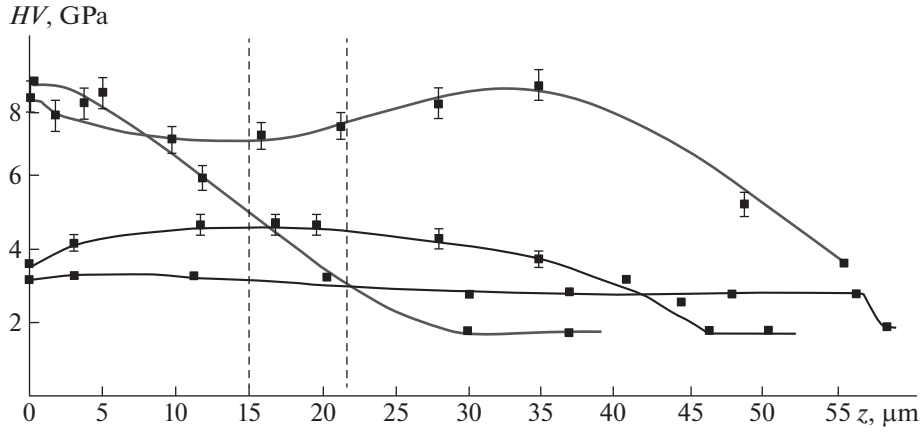

Fig. 2. Microhardness distribution over steel 45 hardened layers after electroexplosive aluminizing and subsequent EBP. The numbers of EBP pulses: (*1*) $N = 10$, (*2*) $N = 30$. (*3*) 200, (*4*) initial sample. The dashed lines show (at the left) the alloying zone boundary and (at the right) the heat affected zone after EEA.

aluminizing with silicon carbide, the microhardness at the surface is 11.1 GPa at the alloying zone depth of 20 μm and the heat affected zone depth 15 μm.

Comparing these values to each other, it should be noted that, when using the powder weights, first, the hardening zone depth and, second, its level increase. In this connection, we note that, when using the powder weights, the increase in the hardening depth after the two-component EEA as compared to the one-component EEA correlates with marked suppression of the radial melt flow from the alloying zone center to its periphery observed as before so in this work. On the other hand, the increase in the microhardness level by factors of 1.3–1.7 should be associated with the formation of new strengthening phases in the alloying zone.

EBP of the EEA steel surface in the case of the optimum conditions of electron beam processing (20 J/cm^2, 50 μm, 0.3 Hz, 10 pulses) leads to insignificant decrease in the microhardness of the steel surface microhardness after EEA (Fig. 2). As the number of EBP pulses increases, the microhardness decreases monotonically and the increased microhardness zone depth increases, achieving 55–60 μm. In this connection, it should be noted that the steel aluminizing by the method of the traditional thermochemical treatment, which is characterized by long-term (for some hours) saturation of surface layers with aluminum at high temperatures, allows us to obtain protective layers with thickness 20–30 μm. The decrease in the microhardness with the increase in the depth is monotonic, except the case of EBP by ten pulses as the microhardness peak of 8.8 GPa observed at a depth about 35 μm is even higher than that at the surface.

EBP of the Boroaluminizing Surface

The distribution of the microhardness over the depth of surface layers of steel 45 after electroexplosion boroaluminizing shows that the combined treatment is accompanied by the formation of the hardening zone, the surface microhardness of which is higher than the microhardness in the steel bulk by a factor of almost 7 (Fig. 3). The increase in the EBP pulse duration from 50 μs (curve *1*) to 200 μs (curve *2*) with the conservation of the surface energy density leads to an increase in the hardened layer thickness by a factor of ~3 at comparable values of the microhardness.

As in the case of EBP of the EEA surface, the increase in the hardening zone depth has engaged our attention, and this increase is much more significant in this case. The depth at which the microhardness is 14–15 GPa is 90 μm. It can be assumed that this fact is related to the increase in the diffusion coefficients of alloying elements, first, boron. Actually, the peculiarity of the processes occurring under action of CEFs on metals is nonequilibrity of the conditions, in which they proceed.

EBP of the Surface Aluminizing with Silicon Carbide

The distribution of the microhardness over the depth of surface layers of steel 45 after electroexplosion aluminizing with silicon carbide shows (Fig. 4) that EBP by mode 1 (Table 1) is accompanied by the formation of a surface layer with relatively low microhardness of 6 GPa as compared to the microhardness on the surface after electroexplosive aluminizing with silicon carbide without EBP that achieves the value 11.8 GPa. As follows from the analysis of the peculiarities of the structural–phase state of the surface layers, in this case the relative low microhardness in the surface layer is due to the formation of the structure of crystallization cells based on γ-Fe and the absence of the influence of the steel quenching for martensite on the results.

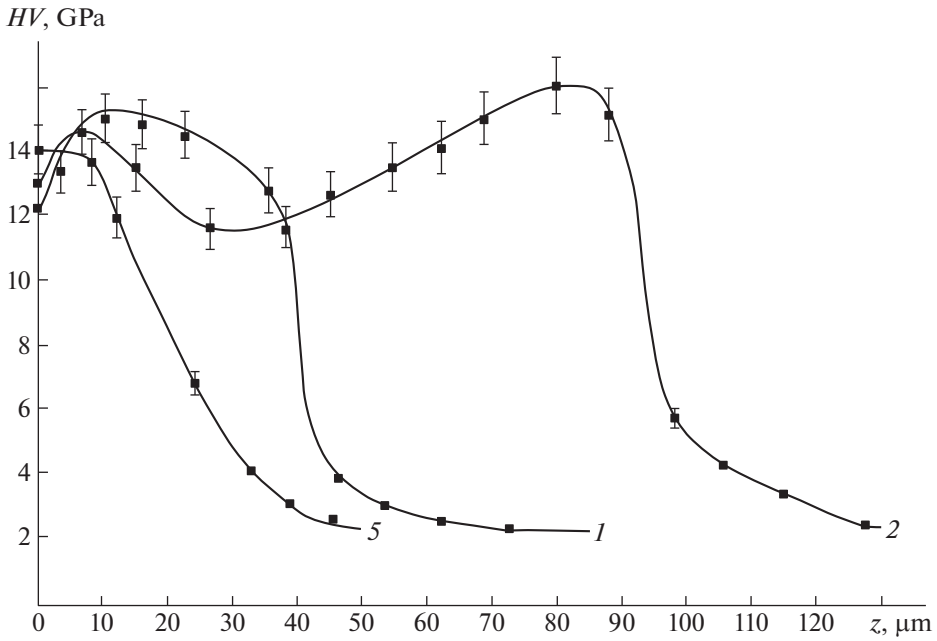

Fig. 3. Microhardness distribution over electroexplosive boroaluminizing zone depth and subsequent EBP of steel 45: (*1*) EBP, mode 1; (*2*) EBP, mode 2; (*3*) electroexplosive aluminizing without EBP.

Going away the processing surface, we observe two microhardness maxima with values 11.0 GPa and 11.1 GPa in the layers located on depths of 3 and 10 μm, respectively. At depth 8 μm, the microhardness decreases to 9.5 GPa. The first microhardness maximum is due to the substitution of the cellular crystallization structure with a grain structure with distance from the processing surface. The grain bulk contains the martensite in which the transverse crystal sizes are changed within 50–100 nm. The decrease in the microhardness with the depth is due to the fact that the dendrite crystallization structure is substituted with the crystallization cell structure based on γ-iron. The second microhardness maximum is due to the formation of particles of iron aluminides, silicon alumocarbides, the existence of particles of the initial silicon carbide powder, high defect structure level (high dislocation density) and the formation of the solid solution of aluminum and silicon i9n crystal lattices on the base of γ-Fe and α-Fe.

EBP of the surface of electroexplosive aluminizing with silicon carbide of steel 45 by mode 2 (Table 2) is accompanied by the increase in the surface layer microhardness to 10 GPa. The increase in the microhardness is due to the formation of the nanosized dendrite crystallization structure on the base of the Fe_3Si phase. In addition, the steel microhardness maximum can be due to the formation of particles of iron aluminide, silicon alumocarbide, the existence of particles of the initial silicon carbide powder, high dislocation density and the formation of the solid solution of aluminum and silicon in crystal lattices on the base of γ-Fe and α-Fe.

It should be noted that, in this case, the hardening zone depth also increases by a factor of almost two. This increase is lower than that in the case of process-

Table 1. Types and modes of combined treatment of steel 45

Hardened material	Types of combined treatment	Optimized processing modes
Steel 45 in annealed state	Electroexplosive boroaluminizing and subsequent electron-beam processing	EEA: $q = 4.5$ GW/m^2, $\tau = 100$ μs. EBP: Mode 1: $q = 4$ GW/m^2, $\tau = 50$ μs, $N = 10$. Mode 2: $q = 1$ GW/m^2, $\tau = 200$ μs, $N = 10$.
	Electroexplosive aluminizing with silicon carbide and subsequent electron-beam processing	EEA: $q = 4.5$ GW/m^2, $\tau = 100$ μs. EBP: Mode 3: $q = 7$ GW/m^2, $\tau = 50$ μs, $N = 10$. Mode 4: $q = 5$ GW/m^2, $\tau = 50$ μs, $N = 5$.

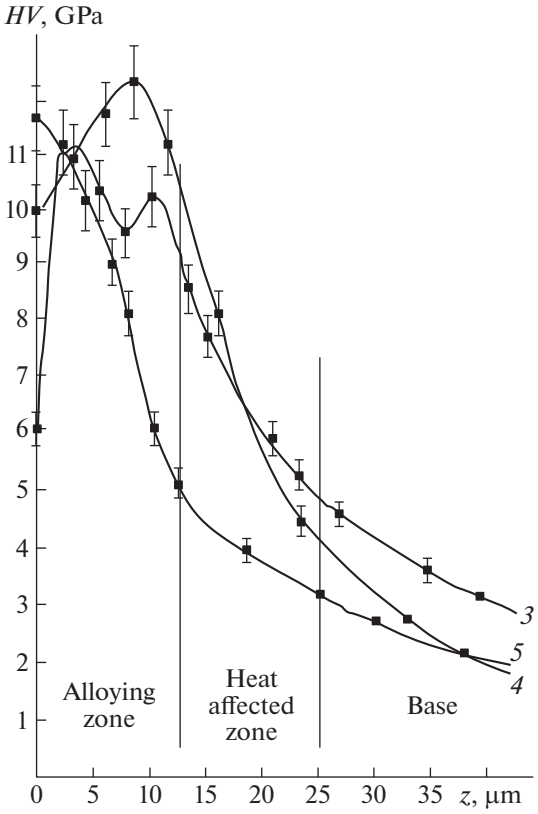

Fig. 4. Microhardness distribution over electroexplosive boroaluminizing combined with silicon carbide zone depth and subsequent EBP of steel 45: (*1*) EBP, mode 1; (*2*) EBP, mode 2; (*3*) electroexplosive aluminizing with silicon carbide without EBP.

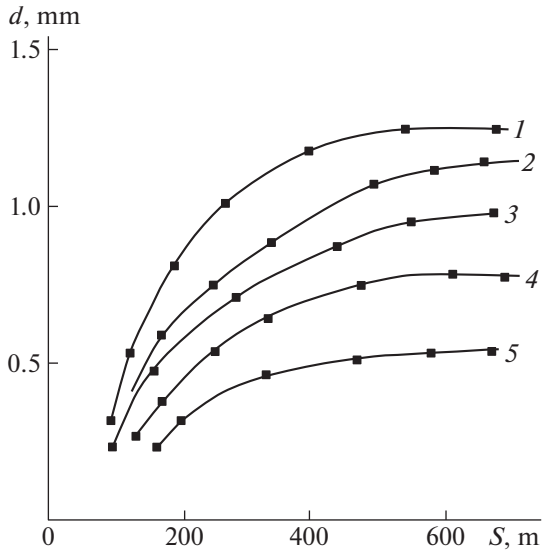

Fig. 5. Increase in the steel 45 wear resistance after boroaluminizing, aluminizing with silicon carbide and combined processing: (*1*) initial sample, (*2*) after electroexplosive aluminizing with silicon carbide, (*3*) after electroexplosive boroaluminizing, (*4*) after electroexplosive aluminizing with silicon carbide and EBP, (*5*) after electroexplosive aluminizing and EBP.

ing of the boroaluminizing surface and shows that the main contribution to this effect is due to diffusion, first, boron [14–16].

The results of measurements of the wear resistance in conditions of wearing without any lubricant showed that the electroexplosive aluminizing with silicon carbide of steel 45 leads to the increase in the wear resistance by a factor of approximately 1.7 and the electroexplosive boroaluminizing, by a factor of 2.4. Additional EBP increases the wear resistance by a factor of 12 in the first case and additionally by a factor of 43 in the second case (Fig. 5). Comparing these results with the data on the microhardness of the EBP surface, we can note their direct correlation: the higher the microhardness, the higher is wear resistance. The surface layers have the maximum wear resistance after electroexplosive boroaluminizing and subsequent EBP.

Heat Model

To simulate the peculiarities of thermal processes during electro-beam action on the metal surface and to find the time dependence of the temperature distribution $T = T(z, t)$, we use the approach based on the concept of the generalized solution. It is in the use of the principle of conservation of energy when enthalpy $U(T)$ immediately enters the equation. In pure substances, at the phase transition temperature, the enthalpy is changed stepwise by the infinite value of the phase transition heat L. In this case the dependence of U on T is ambiguous. For alloys, as a rule, the two-phase zone exists between the solidus T_S and liquidus T_L temperatures, where U is complexly dependent on the phase fractions. In this connection, we introduce the effective specific heat

$$C_e = \frac{L}{(T_L - T_S)}. \tag{4.1}$$

Then the $U(T)$ dependence becomes an unambiguous function and can be given by the following relationships:

$$U = \begin{cases} \rho_S C_S T, & T < T_S, \\ \rho_S C_S T_S + L\rho_S (T - T_S)/(T_L - T_S), & T_S < T < T_L, \\ \rho_S C_L (T - T_L) + \rho_S (L + C_S T_S), & T > T_L, \end{cases} \tag{4.2}$$

where C_S, C_L are specific heats, ρ_S and ρ_L are the densities of the solid and liquid steel, respectively.

We represent the law of changes in the energy taking into account that heat flux q is expressed by the Fourier law in the coordinate form

$$\frac{\partial T}{\partial t} = \frac{\partial}{\partial z}\left(\lambda \frac{\partial T}{\partial z}\right). \tag{4.3}$$

Here, λ is the thermal conductivity coefficient depending on the aggregate state:

$$\lambda = \begin{cases} \lambda_S, & T \le T_S, \\ \lambda_S + (\lambda_L - \lambda_S)(T - T_S)/(T_L - T_S), & T_S < T < T_L, \\ \lambda_L, & T \ge T_L. \end{cases} \quad (4.4)$$

To find $T(z, t)$, we solve Eq. (4.3) with following boundary and initial conditions

$$-\lambda \frac{\partial T(0,t)}{\partial z} = q(t), \quad \frac{\partial T(l,t)}{\partial z} = 0, \quad (4.5)$$

$$T(x,0) = T_0, \quad (4.6)$$

where l is the sample thickness.

The second condition in Eq. (4.5) implies the absence of the heat flux from the side of the sample back surface.

The heat flux on the irradiated surface is given in the form of the stepped function on time:

$$q(t) = \begin{cases} q, & 0 < t < t_p, \\ 0, & t_p < t < t_0, \end{cases} \quad (4.7)$$

where q is the average value of the heat flux for pulse duration t_p; t_0 is the cycle period.

Because of dependences (4.2) and (4.4), the mathematical problem becomes substantially nonlinear; thus we will solve it numerically. To do this, we perform the discretization in time and space. We determine the temperatures in discrete points $T_i^n = T(ih, n\tau)$, where h, τ are steps in space and time, respectively and i, n are the corresponding number of the layers in time and space. Choose the explicit scheme in time and central differences by the space variable:

$$U_i^{n+1} = U_i^n + S[\lambda_{i+1/2}^n (T_{i+1}^n - T_i^n) - \lambda_{i-1/2}^n (T_i^n - T_{i-1}^n)], \quad 1 \le i \le N_x, \quad 0 \le n \le N_t, \quad (4.8)$$

where

$$U_i^n = U(ih, n\tau), \quad S = \tau/h^2, \quad \lambda_{i+1/2}^n = 0.5\left[\lambda(T_{i+1}^n) + \lambda(T_i^n)\right], \quad \lambda_{i-1/2}^n = 0.5\left[\lambda(T_i^n) + \lambda(T_{i-1}^n)\right], \quad \tau = t_0/N_t, \quad h = l/N_z. \quad (4.9)$$

Here, N_t, N_z are the numbers of steps in time and in space, respectively.

To calculate by Eq. (8), it is necessary to know the values of T_0^n and T_{Nz+1}^n. We find these values using boundary conditions (5) written in discrete form:

$$T_0^n = T_1^n + hq(n\tau)/\lambda(T_1^n), \quad T_{Nz+1}^n = T_{Nz}^n. \quad (4.10)$$

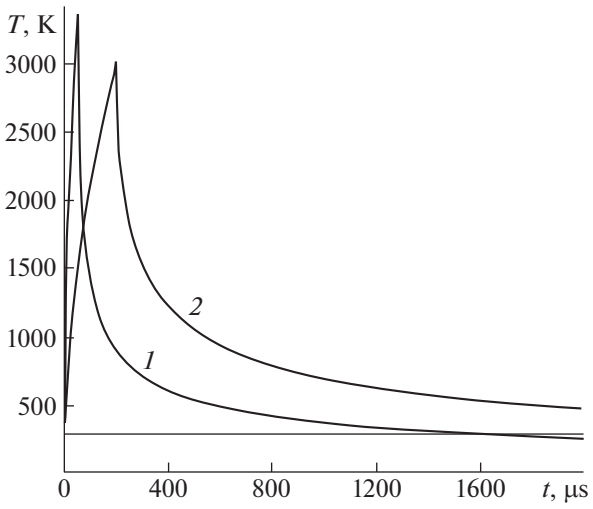

Fig. 6. Kinetic dependences of the temperature change on the surface of technically pure iron after single electron-beam exposure in modes 1 and 2: (*1*) $q = 4$ GW/m^2, $\tau = 50$ μs; (*2*) $q = 1$ GW/m^2, $\tau = 200$ μs. The horizontal line corresponds to room temperature.

We solve the problem (8, 10) numerically for the case of EBP of technically pure iron surface. In this case, we use the following values: $L = 2 \times 10^7$ J/kg, $\rho_S = \rho_L = 7.8 \times 10^3$ kg/m^3, $C_S = C_L = 400$ J/(kg K), $\lambda_S = \lambda_L = 30$ W/(m K), $T_S = 1713$ K, $T_L = 1810$ K, $q = 1$ GW/m^2, and $t_i = 2 \times 10^{-4}$ s.

Figures 6 and 7 show the calculated dependence of temperature $T = T(z, t)$. It is seen that in the modes corresponding to modes 1 and 2 of electroexplosive boroaluminizing surface: (1) $q = 4$ GW/m^2, $\tau = 50$ μs, $N = 10$; (2) $q = 1$ GW/m^2, $\tau = 200$ μs, $N = 10$), the surface is heated to the boiling temperature (taking into account its value at a decreased pressure in the technological chamber of the "SOLO" installation. In this case, the cooling time to room temperature is a fraction of millisecond; thus, we can assume that the individual heat pulses do not influence each other.

The increase in the pulse duration from 50 μs to 200 μs at the same surface energy density leading to the decrease in the heat effect intensity by a factor of four (from 4 to 1 GW/m^2) causes the increase in the melting depth of the surface layer by a factor of 2.7 (Fig. 6). This fact correlates with the data of the optical microscopy and the measurements of the microhardness, according to which the hardening zone depth increases during the transition from mode 1 to mode 2 (Fig. 3). The melting depth also increases as the surface energy density increases at a constant pulse duration, i.e., with an increase in the action intensity. However, in this case, it is evident that intense processes of evaporation from the surface are developed. This evaporation can lead to the loss of alloying elements when processing the metal and alloy surfaces

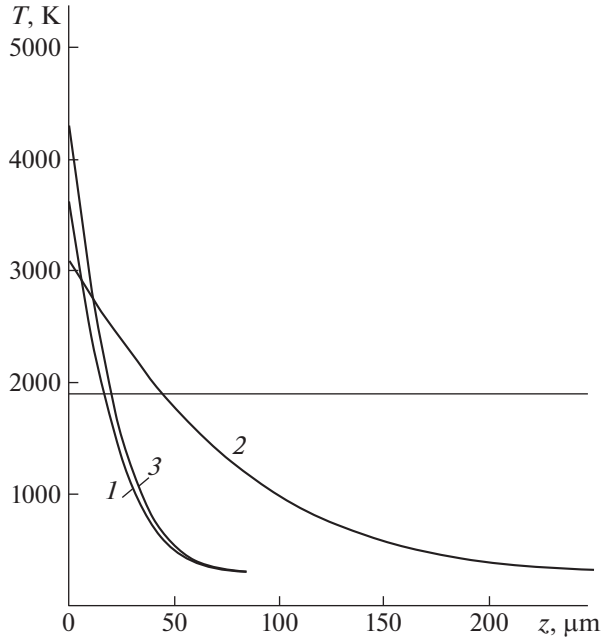

Fig. 7. Calculated dependence of temperature on the surface layer depth at the end of EBP of the technically pure iron surface at single exposure pulse: (*1*) $q = 4$ GW/m^2, $\tau = 50$ μs; (*2*) $q = 1$ GW/m^2, $\tau = 200$ μs; (*3*) $q = 5$ GW/m^2, $\tau = 50$ μs. The horizontal line corresponds to the metal melting temperature.

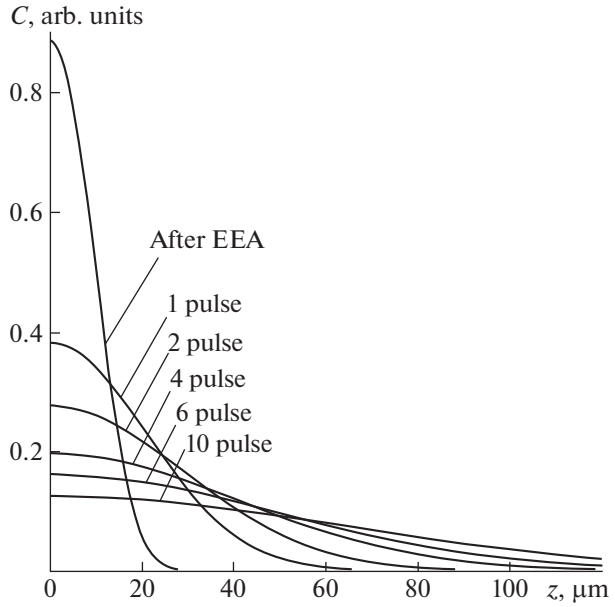

Fig. 8. Dependences of the distribution of alloying element concentration over the depth after processing with different numbers of EBP pulses.

after EEA. The observed decrease in the microhardness measured from the surfaces of obtained samples relative to its level in the bulk, i.e., the formation of the bulk maximum (Fig. 3) can be related namely with the process of evaporation of alloying elements [16].

The Diffusion Model

Not going into the accelerated mass transfer mechanisms, we will assume that, as a result of heat effect on metals below the melted layer, a nonequilibrium state characterizing by the diffusion coefficient of 10^{-2} cm^2/s appears. Consider the mathematical model of the evolution of the concentration field of alloying elements (first, boron) which there are in the surface layer 15–20 μm thick after EEA.

The mathematical problem is to find the concentrations satisfying the diffusion equation, boundary conditions corresponding to the absence of the delivery of diffusing substance from the boundaries and to the initial conditions reflecting the alloying after EEA:

$$\frac{\partial c}{\partial t} = D\frac{\partial^2 c}{\partial z^2}, \quad 0 < z < l, \quad t > 0;$$
$$\frac{\partial c(0,t)}{\partial z} = \frac{\partial c(l,t)}{\partial z} = 0; \quad c(z,0) = \begin{cases} c_0, & 0 < z < h; \\ 0, & z > h, \end{cases} \tag{4.11}$$

where h is the EEA zone thickness, c and c_0 are the concentrations of a diffusing element at the instant of time t and immediately after EEA, respectively.

In the subsequent consideration, the value of c_0 has no principal significance, since we are interesting in the penetration of a diffusion substance in the depth for various instants of time. We will find the solution of problem (4.11) analytically, introducing new variable $u(z, t) = c_z(z, t)$. Then, Eq. (11) takes the form

$$u_t = Du_{zz}, \quad u(0,t) = u(l,t) = 0;$$
$$u(z,0) = c_0[\delta(z) + \delta(z-h)], \tag{4.12}$$

where $\delta(z)$ is the Dirac delta-function. We obtain the solution of problem (4.12) substituting the delta-function in formula:

$$u(z,t) = \frac{2c_0}{l}$$
$$\times \sum_{k=1}^{\infty} \exp\left(-\frac{k^2\pi^2 D}{l^2}t\right)\sin\left(\frac{k\pi z}{l}\right)\sin\left(\frac{k\pi h}{l}\right), \tag{4.13}$$

where k is the summation parameter.

Quantity c_0 has no principal value, since we are interesting in the penetration of the diffusing substance in the depth for various instants of time. In Eq. (4.13), we restrict a finite number of the members of the series denoting it by K. The performed calculations showed that $K = 50$ is sufficient for accuracy calculations.

The series of the dependences shown in Fig. 8 demonstrates the penetration of the concentration profiles in the depth. This penetration can be

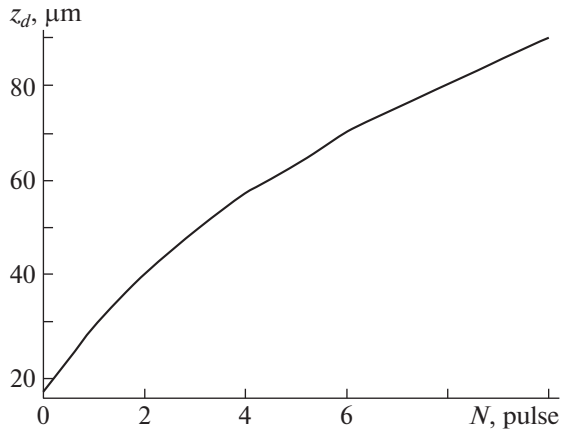

Fig. 9. Calculated dependence of the inflection point of the alloying element concentration profile on the number of EBP pulses.

described most correctly following a certain point on the dependence of $C(x, t)$ on N. We take the inflection point as this certain point and assume that the diffusion penetration front is related to the inflection point motion at the dependence of concentration $C(x, t)$ on N at fixed instants of time.

It is seen (Fig. 9) the penetration depth of alloying elements monotonically increases with the number of electron-beam pulses and achieves the value 90 μm after ten pulses (in this case, the total processing time $t = 2000$ μm). This value corresponds to the penetration depth increase observed experimentally (Fig. 3). This fact counts to favor of the choice of the mechanism of the concentration front penetration on the base of accelerated mass transfer.

Thus, the proposed mathematical models of the heat and mass transfer allow us to explain main peculiarities of the pulse–periodic EBP of the surface of electroexplosive alloying of metals and alloys.

CONCLUSIONS

(1) The combined processing leads to the growth of the hardening depth. After the electroexplosive boroaluminizing and EBP, the microhardness is 16 GPa and the hardening depth is 90 μm; after the electroexplosive aluminizing combined with silicon carbide and EBP, the microhardness is 2 GPa. the wear resistance under conditions of dry sliding friction increases by a factor of 43 after electroexplosive boroaluminizing and EBP and by a factor of 12 at the electroexplosive aluminizing with silicon carbide. The surface hardening is reached due to the formation of the fine-disperse nonequilibrium structure containing strengthening phases.

(2) The models developed in this work allow us to explain the obtained results by the peculiarities of proceeding thermal and diffusion processes at EBP.

ABBRIVIATIONS AND NOTATION

EPO	electron beam processing;
CEF	concentration energy flux;
EEA	electroexplosive alloying;
LEHCEB	low-energy high-current electron beam;

FUNDING

This work was supported by ongoing institutional funding. No additional grants to carry out or direct this particular research were obtained.

CONFLICT OF INTEREST

The author of this work declares that she has no conflicts of interest.

REFERENCES

1. V. A. Shulov, A. B. Belov, and A. F. L'vov, Fiz. Khim. Obrab. Mater., No. 2, **61** (2005).
2. A. Ya. Bagautdinov, E. A. Budovskikh, Yu. F. Ivanov, and V. E. Gromov, *Physical Bases of Electroexplosive Alloying of Metals and Alloys* (SibGIU, Novokuznetsk, 2007) [in Russian].
3. A. V. Ionina and E. A. Budovskikh, Prikl. Fiz. Mat., No. 2, 3 (2023). https:// https://doi.org/10.25791/pfi m.02.2023.1253
4. D. V. Komarov, S. V. Konovalov, I. A. Panchenko, and E. A. Timofeeva, in: *Proceedings of the International Scientific and Practical Conference*, Ed. by V. E. Gromov (SibGIU, Novokuznetsk, 2021), p. 109 [in Russian].
5. A. V. Vostretsova, Yu. F. Ivanov, and S. Yu. Filimonov, Izv. Vyssh. Uchebn. Zaved., Fiz., No. 11/2, 161 (2009).
6. Yu. F. Ivanov, Yu. A. Kolubaeva, and S. Yu. Filimonov, Izv. Vyssh. Uchebn. Zaved., Chern. Metall., No. 12, 43 (2008).
7. Yu. F. Ivanov, Yu. A. Kolubaeva, and S. Yu. Filimonov, Uprochnyayushchie Tekhnol. Pokrytiya, No. 2, 17 (2009).
8. Yu. F. Ivanov, Yu. A. Kolubaeva, and S. Yu. Filimonov, Izv. Vyssh. Uchebn. Zaved., Chern. Metall., No. 10, 42 (2009).
9. Yu. F. Ivanov, S. Yu. Filimonov, and Yu. A. Kolubaeva, Fundam. Probl. Sovrem. Materialoved., No. 2, 119 (2009).
10. S. V. Karpii, M. M. Morozov, and Yu. F. Ivanov, Izv. Vyssh. Uchebn. Zaved., Chern. Metall., No. 8, 42 (2010).
11. S. V. Karpii, M. M. Morozov, and E. A. Budovskikh, Usp. Fiz. Met. **11**, 1 (2010).
12. S. V. Karpii, Yu. F. Ivanov, and N. N. Koval, Fiz. Khim. Obrab. Mater., No. 4, **24** (2010).

13. A. G. Kolmakov, V. F. Terent'ev, and M. B. Bakirov, *Methods for Measuring Hardness: A Reference Guide* (Intermet Inzhiniring, Moscow, 2005) [in Russian].

14. D. V. Zagulyaev, Yu. F. Ivanov, A. A. Abaturova, A. M. Ustinov, and V. E. Gromov, in: *Physical Materials Science. Current Problems of Strength. Proceedings of the X International School Dedicated to the 10th Anniversary of the Laboratory of Physics of Strength and Intelligent Diagnostic Systems and the LXIII International Conference* (Togliatti, 2021), p. 106 [in Russian].

15. A. V. Ionina, Inzh. Fiz., No. 12, 17 (2022).

16. A. V. Ionina, in: *KoMU-2022: Proceedings of the XIV All-Russian School–Conference of Young Scientists with International Participation, Izhevsk, December 05–09, 2022* (FGBUN Udmurt. Fed. Issled. Tsentr Ural. Otd. Ross. Akad. Nauk, Izhevsk, 2022), p. 127 [in Russian].

Translated by Yu. Ryzhkov

SPELL: OK